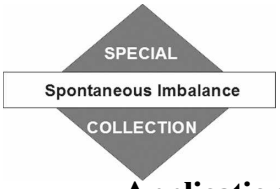

Application of the Lighthill–Ford Theory of Spontaneous Imbalance to Clear-Air Turbulence Forecasting

JOHN A. KNOX

Department of Geography, University of Georgia, Athens, Georgia

DONALD W. MCCANN

McCann Aviation Weather Research, Inc., Overland Park, Kansas

PAUL D. WILLIAMS

Department of Meteorology, University of Reading, Reading, United Kingdom

(Manuscript received 23 March 2007, in final form 15 November 2007)

ABSTRACT

A new method of clear-air turbulence (CAT) forecasting based on the Lighthill–Ford theory of spontaneous imbalance and emission of inertia–gravity waves has been derived and applied on episodic and seasonal time scales. A scale analysis of this shallow-water theory for midlatitude synoptic-scale flows identifies advection of relative vorticity as the leading-order source term. Examination of leading- and second-order terms elucidates previous, more empirically inspired CAT forecast diagnostics. Application of the Lighthill–Ford theory to the Upper Mississippi and Ohio Valleys CAT outbreak of 9 March 2006 results in good agreement with pilot reports of turbulence. Application of Lighthill–Ford theory to CAT forecasting for the 3 November 2005–26 March 2006 period using 1-h forecasts of the Rapid Update Cycle (RUC) 2 1500 UTC model run leads to superior forecasts compared to the current operational version of the Graphical Turbulence Guidance (GTG1) algorithm, the most skillful operational CAT forecasting method in existence. The results suggest that major improvements in CAT forecasting could result if the methods presented herein become operational.

1. Introduction

The theory of spontaneous imbalance owes its origins to Lighthill's (1952) study of aerodynamically generated sound waves and Ford's (1994) extension of the problem to rotating shallow-water flow and inertia–gravity wave generation. In their analyses, the waves are emitted spontaneously by the vortical flow. This characteristic distinguishes the spontaneous imbalance problem from the initial value imbalance and gravity wave generation of "geostrophic adjustment" (Rossby 1938; Cahn 1945) and from boundary condition perturbations leading to topographically forced gravity waves (Smith 1979). Instead, it is fundamentally rooted in the "universal 'internal' . . . nonlinearity of atmospheric motions," as demonstrated by Medvedev and Gavrilov (1995) in their independent extension of Lighthill's theory.

While the weakness of spontaneous emission in Lighthill–Ford theory is sometimes emphasized, in this paper we stress the fact that the theory does indeed predict gravity wave radiation, even at an arbitrarily small Rossby number (Ford et al. 2000). Even weak gravity waves can have sizable impacts on the background flow (Williams et al. 2003). In this paper, we emphasize that weak gravity waves can modify the local environmental stability and wind shear to reduce the Richardson number (section 6.3 of Nappo 2003) to values that allow for turbulence production (Roach 1970; McCann 2001).

Gravity wave radiation is therefore of particular importance to the study and forecasting of clear-air turbulence (CAT). CAT is in-flight bumpiness detected by aircraft at high altitudes in regions devoid of significant

Corresponding author address: Dr. John A. Knox, Department of Geography, University of Georgia, Athens, GA 30602.
E-mail: johnknox@uga.edu

DOI: 10.1175/2008JAS2477.1

cloudiness or nearby thunderstorms. Much of this bumpiness is assumed to be caused by aircraft flying in or near gravity waves (Ellrod et al. 2003). Commercial aircraft encounter severe, or greater, turbulence about 5000 times each year, the majority of which occur above flight levels 10 000 ft above mean sea level (FL100); these incidents lead to tens of millions of dollars in injury claims per year (Sharman et al. 2006). However, a significant limitation for the forecasting of all types of aviation turbulence is identifying the source of gravity waves (McCann 2001). Partly as a result, current federal goals for aviation turbulence forecasting are "currently not achievable by either automated or experienced human forecasters" (Sharman et al. 2006).

In the case of CAT, a candidate source of these waves is spontaneous imbalance. Observational experience (e.g., Sorenson 1964) has long indicated the following two flow regimes associated with CAT: strongly cyclonic and strongly anticyclonic flows. Cyclonic CAT has been explained and predicted with some success via Kelvin–Helmholtz instability theory (Dutton and Panofsky 1970) related to frontogenesis and deformation (e.g., Ellrod and Knapp 1992). These regions sometimes correspond to areas in which spontaneous emission of gravity waves is expected to occur (e.g., fronts and jets). Occurrences of CAT in strongly anticyclonic flows are rarer but also more problematic to forecast (Knox 1997). A recent work in progress (G. P. Ellrod and J. A. Knox 2008, unpublished manuscript) suggests that augmenting usual deformation/vertical shear forecast methods with divergence tendency leads to improved prediction methods, particularly in anticyclonic regions. In this context, it is of interest that Ford (1994) found the strongest spontaneous gravity wave generation in strongly anticyclonic regions of zero or negative potential vorticity. In summary, CAT forecasting remains an unsolved problem (McCann 2001) for spontaneous imbalance theory to address.

Williams et al. (2005) employed laboratory experiments and a quasigeostrophic model's results to explore generation mechanisms of gravity waves in a rotating, two-layer vertically sheared flow. To diagnose wave activity, the authors calculated five dynamical indicators, several of which were originally devised as CAT forecasting indices (Roach 1970; Brown 1973). The most accurate indicator tested by Williams et al., however, derived from Lighthill–Ford theory. Williams et al. concluded, "Further work is required to determine in more detail how to properly interpret the Lighthill/Ford indicator," its "geophysical relevance and applicability," and its relationship to other indicators of imbalance. This is the motivation for the present work.

This work is organized as follows. In section 2 we derive an applications-friendly version of the Lighthill–Ford theory, and discuss each forcing term and the relationship of the leading-order terms to established CAT forecasting techniques. In section 3 the method used to apply this theory as a CAT forecasting tool is explained. In section 4 a case study is presented showing the utility of Lighthill–Ford theory in CAT forecasting. Section 5 examines a season-long database that demonstrates the superiority of applying this theory versus other CAT forecasting methods, and discussion and concluding remarks are provided in section 6.

2. Theory

a. Derivation

Lighthill (1952) derived the theory for the generation of sound waves by large-scale motions in a three-dimensional compressible adiabatic gas. With extension to nonrotating shallow-water flow, Lighthill's theory predicts pure gravity wave generation. Ford (1994) extended this theory to rotating stratified flow and inertia–gravity wave generation, as did Medvedev and Gavrilov (1995). We are not aware of an extant extension of this theory to the baroclinic case.

Ford's derivation is based on the flux forms of the momentum and conservation of mass equations in shallow-water flow on the f plane. By forming the divergence and vorticity equations, and then combining them with conservation of mass and its second derivative, Ford obtained the following wave equation:

$$\left(\frac{\partial^2}{\partial t^2} + f^2 - gh_0\nabla^2\right)\frac{\partial h}{\partial t} = \frac{\partial^2}{\partial x_i \partial x_j} T_{ij}, \tag{1}$$

in which g is the acceleration due to gravity, h is the layer depth, and h_0 is the layer depth far from the region of vortical motion; in standard tensor notation T_{ij} is

$$T_{ij} = \frac{\partial}{\partial t}(hu_i u_j) + \frac{f}{2}(\varepsilon_{ik} hu_j u_k + \varepsilon_{jk} hu_i u_k) + \frac{1}{2} g \frac{\partial}{\partial t}(h - h_0)^2 \delta_{ij}. \tag{2}$$

Ford (1994) and Williams et al. (2005) indicated that nonzero values on the right-hand side of (1) should be regarded as a source of gravity waves. Strictly speaking, this interpretation is not exact because the variable h is not isolated on the left-hand side of (1). However, the separation of time scales and the weakness of the gravity waves compared to the large-scale flow allow for this interpretation, and this interpretation has also been confirmed by Williams et al.'s laboratory experiments.

Williams et al. (2005) referred to the right-hand side of (1) as the "Lighthill/Ford radiation term" and reexpressed it as

$$R = \underbrace{\frac{\partial}{\partial t}(\boldsymbol{\nabla}\cdot\mathbf{G})}_{\text{Term 1}} + \underbrace{f\mathbf{k}\cdot\boldsymbol{\nabla}\times\mathbf{G}}_{\text{Term 2}} + \underbrace{\frac{g}{2}\frac{\partial}{\partial t}\nabla^2(h-h_0)^2}_{\text{Term 3}}, \quad (3)$$

in which

$$\mathbf{G} = \mathbf{u}\boldsymbol{\nabla}\cdot(h\mathbf{u}) + (h\mathbf{u}\cdot\boldsymbol{\nabla})\mathbf{u}. \quad (4)$$

(Note that Williams et al. expressed term 3 as a function of h instead of $h - h_0$, but we choose the latter to maintain consistency with Ford's theory.)

These expressions for Lighthill–Ford radiation are not convenient for interpretation and application. As an extension of previous work, therefore, we expand each term in (3) and discuss each term separately regarding its contribution to spontaneous imbalance. [Derivatives of h arising from (4) may be shown to sum to zero via conservation of mass; we omit them below.]

Term 1 can be expressed as a function of a common diagnostic of imbalance, the horizontal divergence D:

$$\frac{\partial}{\partial t}(\boldsymbol{\nabla}\cdot\mathbf{G}) = 2h\left[\underbrace{\frac{\partial}{\partial t}D^2}_{\text{Term 1A}} + \underbrace{\frac{\partial}{\partial t}\mathbf{u}\cdot\boldsymbol{\nabla}D}_{\text{Term 1B}} - \underbrace{\frac{\partial}{\partial t}J(u,v)}_{\text{Term 1C}}\right]. \quad (5)$$

These subterms are obtained from the time derivative of the divergence equation in the derivation of (1). Term 1A is a source term resulting from the local change of divergence; term 1B is a source of gravity waves via the local change of the horizontal advection of horizontal divergence; and term 1C is the time derivative of the familiar Jacobian term found in both the divergence equation and in its approximated form, the nonlinear balance equation (NBE; Zhang et al. 2000).

Term 2 is expressible as a combination of the horizontal divergence and the vertical component of relative vorticity ζ:

$$f\mathbf{k}\cdot\boldsymbol{\nabla}\times\mathbf{G} = h\left[\underbrace{2Df\zeta}_{\text{Term 2A}} + \underbrace{f\mathbf{u}\cdot\boldsymbol{\nabla}\zeta}_{\text{Term 2B}} + \underbrace{f\left(v\frac{\partial D}{\partial x} - u\frac{\partial D}{\partial y}\right)}_{\text{Term 2C}}\right]. \quad (6)$$

The product of divergence, planetary vorticity, and relative vorticity is found in term 2A; this product is not found elsewhere in the divergence, NBE, or vorticity equations. Term 2B is proportional to the horizontal advection of relative vorticity. Term 2C is proportional to the vertical component of the cross product of the vector velocity with the horizontal gradient of divergence.

Term 3 can also be reexpressed as

$$\begin{aligned}\frac{g}{2}\frac{\partial}{\partial t}\nabla^2(h-h_0)^2 &= g\nabla^2\left[(h-h_0)\frac{\partial(h-h_0)}{\partial t}\right]\\ &= g\left[\underbrace{\frac{\partial h}{\partial t}\nabla^2 h}_{\text{Term 3A}} + \underbrace{(h-h_0)\left(\nabla^2\frac{\partial h}{\partial t}\right)}_{\text{Term 3B}}\right.\\ &\quad \left.+ \underbrace{2\left(\frac{\partial h}{\partial x}\frac{\partial^2 h}{\partial t\partial x} + \frac{\partial h}{\partial y}\frac{\partial^2 h}{\partial t\partial y}\right)}_{\text{Term 3C}}\right]. \quad (7)\end{aligned}$$

In term 3A, the Laplacian of height appears, reminiscent of the Laplacian of geopotential found in the divergence and NBE equations.

b. Scale analysis

Following Haltiner and Williams (1980, 54–59), a simple scale analysis of the Lighthill–Ford radiation subterms in (5), (6), and (7) can be performed for synoptic-scale midlatitude flows with small Rossby number (Ro $\ll 1$), background conditions that in our experience are representative of many clear-air turbulence outbreaks.

Assuming velocity and length scales of U and L, an advective time scale, and that the ratio of divergent and rotational components of the velocity scales as Ro, then

$$T \sim \frac{L}{U}, \quad \zeta \sim \frac{U}{L}, \quad \text{and} \quad D \sim \mathrm{Ro}\,\frac{U}{L}. \quad (8)$$

In addition, by invoking the definition

$$f \equiv \frac{1}{\mathrm{Ro}}\frac{U}{L}, \quad (9)$$

we can scale terms 1 and 2 with respect to (nonzero) Ro:

$$\frac{\partial}{\partial t}(\boldsymbol{\nabla}\cdot\mathbf{G}) \sim \frac{U^3}{L^2}\left[\underbrace{\mathrm{Ro}^2}_{\text{Term 1A}}\ \underbrace{\mathrm{Ro}}_{\text{Term 1B}}\ \underbrace{1}_{\text{Term 1C}}\right], \quad (10)$$

$$f\mathbf{k}\cdot\boldsymbol{\nabla}\times\mathbf{G} \sim \frac{U^3}{L^2}\left[\underbrace{1}_{\text{Term 2A}}\ \underbrace{\mathrm{Ro}^{-1}}_{\text{Term 2B}}\ \underbrace{1}_{\text{Term 2C}}\right]. \quad (11)$$

To leading order for Ro $\ll 1$, therefore,

$$\frac{\text{Term 1}}{\text{Term 2}} \propto \frac{\text{Term 1C}}{\text{Term 2B}} \sim \mathrm{Ro}. \quad (12)$$

This result agrees with Williams et al.'s (2005) comment that the ratio of terms 1 and 2 should scale as the bulk

Rossby number. We have, however, extended their results and identified the leading-order components within terms 1 and 2 that lead to that scaling. We also confirm for low Ro their speculation that only term 2 might be retained for "many practical purposes." Additionally, Medvedev and Gavrilov's (1995) analysis emphasized the equivalent of our term 2B for inertia–gravity wave forcing by quasigeostrophic motions.

To scale term 3, we rewrite it in terms of Reznik et al.'s (2001) nonlinearity parameter λ:

$$\frac{g}{2}\frac{\partial}{\partial t}\nabla^2(h-h_0)^2 \sim \frac{U^3}{L^2}\lambda^2. \tag{13}$$

Furthermore, for standard quasigeostrophic conditions, Reznik et al. note that λ scales as Ro. Therefore, for our analysis,

$$\frac{g}{2}\frac{\partial}{\partial t}\nabla^2(h-h_0)^2 \sim \frac{U^3}{L^2}\mathrm{Ro}^2. \tag{14}$$

Thus, for small Ro, term 3 would be similar in magnitude to $O(\mathrm{Ro}^2)$, that is, three orders of magnitude smaller than term 2B. This scaling is broadly consistent with the quasigeostrophic model results of Williams et al. (2005, their Fig. 7), who found term 2 to be a factor of 40 or more larger than term 3, and with Sugimoto et al. (2008), who found term 3 to be negligible even for large Ro.

To summarize, our scale analysis of the Lighthill–Ford radiation terms identifies the following:

- leading-order term: term 2B (advection of relative vorticity);
- second-order terms: term 1C, term 2A, term 2C; and
- third-order and smaller terms: term 1A, term 1B, term 3.

Therefore, we should expect to find that regions of large advection of relative vorticity should be a dominant source of spontaneous gravity wave generation. Medvedev and Gavrilov [1995, their Eq. (23)] also identified advection of relative vorticity as the source term for inertia–gravity waves in their extension of Lighthill's theory.

The Jacobian term, divergence–vorticity product, and cross product of velocity with the gradient of divergence may also play nonnegligible roles for situations in which $\mathrm{Ro} < 1$ but not $\mathrm{Ro} \ll 1$. As a result, we also retain these terms. Medvedev and Gavrilov [1995, their Eq. (18)] identified a source term similar to terms 1A and 1C as the most important for the generation of mesoscale waves.

In the following sections we test these expectations with data from clear-air turbulence observations, with the clear understanding that this theory is designed for shallow-water flow rather than the baroclinic atmosphere.

c. Interpretation

The interpretation of Lighthill–Ford theory in terms of spontaneous imbalance and wave generation affords an opportunity to reexamine previous, often empirically inspired work on clear-air turbulence in light of new and fundamental theory.

The second term of the vector form of the Lighthill–Ford radiation term in (4), $(h\mathbf{u}\cdot\boldsymbol{\nabla})\mathbf{u}$, is essentially identical to the numerator of the advective Rossby number used by Uccellini et al. (1984) to diagnose unbalanced flow. CAT diagnostics based on the advective Rossby number, such as the inertial-advective wind (Knox 2001), and the Lagrangian Rossby number (van Tuyl and Young 1982; Koch and Dorian 1988) have been used with some success in CAT forecasting. Interestingly, the leading-order term of our scale analysis results from this second vector term on the RHS of (4). Thus, the use of inertial-advective CAT predictors may be related to this component of Lighthill–Ford spontaneous gravity wave generation.

The leading-order term 2B has been previously identified as a CAT forecasting diagnostic. Shapiro (1978) related gradients of potential vorticity to CAT; Kaplan et al. (2005) created a CAT predictor related to gradients of relative vorticity. A long-standing rule-of-thumb CAT forecasting technique in the aviation meteorology community has been to identify regions of strong negative absolute vorticity advection (e.g., Sharman et al. 2006, their appendix A, item p). However, during the past four decades deformation and vertical shear, rather than horizontal vorticity advection, have been emphasized in CAT forecasting techniques.

For example, one of the more successful diagnostics of CAT (e.g., Roach 1970; Brown 1973; Dutton 1980; Keller 1990; Ellrod and Knapp 1992) has been flow deformation DEF, defined as

$$\mathrm{DEF}^2 = \left(\frac{\partial u}{\partial x} - \frac{\partial v}{\partial y}\right)^2 + \left(\frac{\partial v}{\partial x} + \frac{\partial u}{\partial y}\right)^2. \tag{15}$$

However, why should flow deformation be related to CAT? Conventional wisdom links DEF to frontogenesis and ultimately to Kelvin–Helmholtz instability. The seminal paper linking CAT and deformation by Mancuso and Endlich (1966) sought instead a link between deformation and the generation of mesoscale waves that could degenerate into turbulence. In 1966 the concept of large deformation triggering mesoscale waves "lack[ed] theoretical support," so Mancuso and Endlich

turned instead to frontogenetical arguments involving vertical wind shear. However, they concluded, "We do not have a completely satisfactory explanation for the physical connection between turbulence and the product of vertical wind shear and deformation."

Lighthill–Ford theory may be able to provide a mesoscale wave generation–deformation linkage that Mancuso and Endlich (1966) sought in vain. One can algebraically equate (without approximation) term 1C to DEF as

$$\frac{\partial}{\partial t}[-2J(u,v)] = \frac{1}{2}\frac{\partial}{\partial t}(\mathrm{DEF}^2 - \zeta^2 - D^2). \quad (16)$$

The D^2 term scales as Ro^2 and is often negligible. Therefore, in regions of small and/or nearly steady relative vorticity,

$$\frac{\partial}{\partial t}[-2J(u,v)] \approx \frac{1}{2}\frac{\partial}{\partial t}(\mathrm{DEF}^2) = \mathrm{DEF}\frac{\partial}{\partial t}(\mathrm{DEF}). \quad (17)$$

Thus, a direct connection can be made (at least in certain circumstances) between flow deformation and inertia–gravity wave generation via Lighthill–Ford theory. This may partially explain the surprising success of deformation-based CAT predictors despite weaknesses in their derivation and application (Knox 1997).

It is also of note that G. P. Ellrod and J. A. Knox (2008, unpublished manuscript) recently introduced a hybrid deformation-based CAT diagnostic that also incorporates the time trend of divergence, specifically to address hard-to-forecast CAT in strongly anticyclonic regions. Its inspiration derives from McCann (2001) and also empirical experience, but the hybrid's success may also be explainable in terms of Lighthill–Ford theory. In the case where DEF and divergence are not negligible and relative vorticity is quasi constant, (16) can be written as

$$\frac{\partial}{\partial t}[-2J(u,v)] \approx \frac{1}{2}\frac{\partial}{\partial t}(\mathrm{DEF}^2 - D^2)$$

$$= \mathrm{DEF}\frac{\partial}{\partial t}(\mathrm{DEF}) - D\frac{\partial D}{\partial t}. \quad (18)$$

Thus, both deformation and the local tendency of divergence can be related to one of the second-order subterms of the Lighthill–Ford gravity wave radiation term. This may provide some theoretical justification for the approach of Ellrod and Knox.

Another second-order term 2A possesses a unique characteristic that was proposed in an earlier paper on CAT. Knox (1997), noting Sparks et al.'s (1977) observations of frequent CAT in both strongly anticyclonic and strongly cyclonic flows, suggested that a parabolic nonlinear relationship between CAT and absolute vorticity might exist, with a minimum at intermediate values of absolute vorticity. The absolute value of term 2A, $2|Df\zeta|$, captures this nonlinearity—assuming large $|D|$ at near-zero absolute vorticity or in regions of large absolute vorticity, a parabolic curve is obtained for $2|Df\zeta|$ as a function of absolute vorticity (not shown).

A popular indicator of imbalance is the residual of the NBE (e.g., Houghton et al. 1981; Moore and Abeling 1988; Zhang et al. 2000). Plougonven and Zhang (2007) recently derived a vertically propagating inertia–gravity wave equation in which the right-hand forcing terms included the Lagrangian derivative of the vertical gradient of the NBE residual. Our analysis of Lighthill–Ford theory for horizontally propagating waves, however, does not reveal a similarly close relationship between wave generation and the NBE residual. Our leading-order radiation term, advection of relative vorticity, is not part of the NBE residual. The second-order term 1C is the time derivative of the Jacobian, which is found in the NBE residual. The second-order term 2A contains $f\zeta$, which is also found in the NBE residual, but in term 2A it is multiplied by D. Terms 1A and 1B are time derivatives of divergence and advection of divergence, which would be nonzero in the event of NBE imbalance. However, these terms are third-order in our Lighthill–Ford scale analysis.

In short, from the perspective of Lighthill–Ford theory the NBE residual does not manifest itself as a significant diagnostic of gravity wave generation indicator. Other quantities discussed in this section appear to be more appropriate. Finally, because Lighthill–Ford theory combines divergence and vorticity equations, whereas the NBE is an approximated form of the divergence equation, it would seem that Lighthill–Ford theory should possess whatever advantages have been gained by using NBE residual as a flow imbalance diagnostic.

In summary, the Lighthill–Ford theory of spontaneous imbalance can be related to several existing clear-air turbulence forecasting approaches of the past 40 years, which were often inspired by empirical, rule-of-thumb approaches.

3. Methods

Having performed a scale analysis of the Lighthill–Ford theory for synoptic-scale midlatitude flows, we now discuss how to implement it as a clear-air turbulence forecasting diagnostic.

We hypothesize that gravity waves spontaneously emitted according to Lighthill–Ford theory relate to clear-air turbulence felt by aircraft in the following

manner. First, the gravity wave acts upon the environment and destabilizes it. If the environment is close to being dynamically unstable with respect to Kelvin–Helmholtz instability (i.e., the environment has small Richardson number Ri), then the gravity wave causes Ri to be reduced locally to less than 0.25 and turbulence ensues (Miles and Howard 1964; Dutton and Panofsky 1970). Therefore, not only Lighthill–Ford forcing but also the environmental Ri must be considered in the production of turbulence. In this way, even weak gravity waves may initiate turbulence.

The intensity of the turbulence is not addressed by either of these two quantities. A separate quantity, turbulent kinetic energy (TKE) dissipation, is the only known quantitative approach that is correlated with aircraft turbulence intensity (McCann 1999; also see "eddy dissipation rate" in Cornman et al. 1995).

For these reasons, we pursue the application of Lighthill–Ford theory as a CAT forecasting diagnostic using the TKE approach of McCann (2001). In this paper, McCann outlined a simple first-order turbulence closure ingredients-based CAT forecast technique and presented a procedure for combining the ingredients. We summarize this procedure below.

To reiterate, the guiding assumption in McCann (2001) is that gravity waves locally modify the environmental Ri, which can then trigger CAT via Kelvin–Helmholtz instability. [This theory fundamentally differs from the Mancuso and Endlich (1966) approach in that gravity waves do not "degenerate" into turbulence. Their theory implies that the turbulence cascade begins at the mesoscale while McCann's implies a much smaller scale.] Because the modified Ri fluctuates within a gravity wave, only portions of the wave may be turbulent. The maxima of the two sources of production of gravity wave–enhanced turbulent kinetic energy may be estimated as

$$\varepsilon_{\text{buoy}} = K_h(\hat{a} - 1)N^2, \tag{19}$$

and

$$\varepsilon_{\text{wshr}} = K_m\left(\frac{\partial \mathbf{V}}{\partial z}\right)^2\left(1 + \hat{a}\sqrt{\text{Ri}}\right)^2. \tag{20}$$

In (19) and (20), $\varepsilon_{\text{buoy}}$ and $\varepsilon_{\text{wshr}}$ are the gravity wave–modified TKE dissipation resulting from buoyancy and wind shear, respectively, K_h and K_m are the eddy thermal diffusivity and the eddy viscosity, respectively, and $\mathbf{V}$ is the vector horizontal wind. The ratio K_m/K_h is a turbulent Prandtl number; the closer this ratio is to 0.25, the less intermittent the turbulence. The eddy viscosity is empirically determined so that the resulting TKE dissipation estimates the eddy dissipation rate of actual aircraft (Cornman et al. 1995). The eddy thermal diffusivity is $K_h = 4K_m$. The Brunt–Väisälä frequency squared is $N^2 = g/\Theta(\partial\Theta/\partial z)$, in which Θ is the potential temperature. The final output of the algorithm is the maximum of (19) and (20).

A key parameter in (19) and (20) is the nondimensional amplitude

$$\hat{a} = Na/|\mathbf{V} - \mathbf{c}|, \tag{21}$$

where a is the actual wave amplitude and $\mathbf{c}$ is the wave phase velocity; it is an inverse Froude number. The nondimensional amplitude denominator is the Doppler-adjusted wind velocity (Dunkerton 1997).

Maximum positive TKE production from buoyancy arises when $\hat{a} > 1$ and from wind shear when

$$\hat{a} > 2 - \text{Ri}^{-1/2}. \tag{22}$$

The method assumes that in the typical forecast time the TKE production eventually cascades into molecular TKE dissipation through the inertial subrange felt by the aircraft. At any one moment an aircraft may feel less than the maximum TKE dissipation because of its position within the gravity wave.

Any type of gravity wave forcing may be implemented, but the method requires knowledge of the wave amplitudes and phase velocities that, for the most part, are unknown. Because of a lack of consensus about the scaling properties of inertia–gravity wave amplitudes in theories and atmospheric observations, we seek guidance from laboratory experiments (Williams et al. 2008). The inertia–gravity waves generated in these experiments have an amplitude that scales linearly with the Rossby number. Noting that the Lighthill–Ford source term varies as Ro^2, we deduce that if atmospheric inertia–gravity waves behave like those in the laboratory, then their amplitude must be proportional to the square root of the leading- and second-order terms in the Lighthill–Ford source term,

$$\hat{a}^2 \propto f\mathbf{u}\cdot\nabla\zeta + 2Df\zeta - f\mathbf{k}\cdot\mathbf{u}\times\nabla D - 2\frac{\partial}{\partial t}J(u, v). \tag{23}$$

We assume constant mean wave properties in (23).

The proportionality constant in (23) was determined empirically by matching distributions of pilot reports of turbulence in strong CAT outbreaks prior to 2005–06 with the patterns of TKE dissipation that fit the best. This constant was then held fixed in the analyses of 2005–06 CAT occurrences discussed in sections 4 and 5 below.

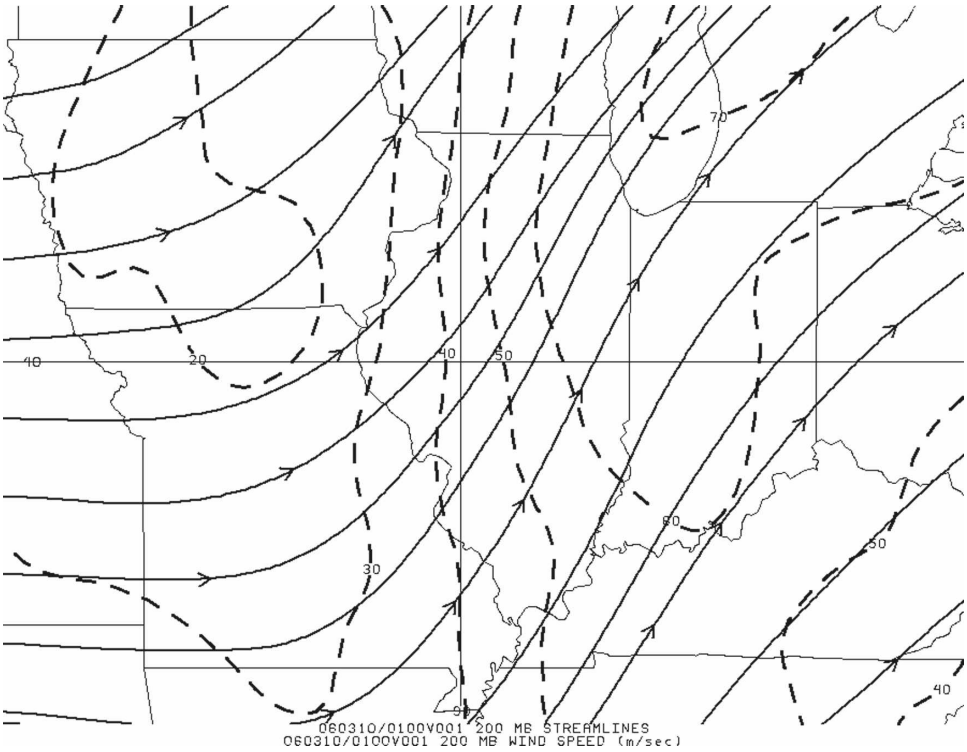

FIG. 1. One-hour RUC2 forecast of the 200-hPa streamlines and wind speed (dashed, m s^{-1}) for the Upper Mississippi and Lower Ohio Valleys, valid at 0100 UTC 10 March 2006.

In the case of term 1C, we compute the instantaneous time derivative of the Jacobian as

$$\frac{\partial}{\partial t} J(u, v) = J\left(\frac{\partial u}{\partial t}, v\right) + J\left(u, \frac{\partial v}{\partial t}\right), \tag{24}$$

with the time derivatives in (23) calculated from the equation of motion via

$$\frac{\partial u}{\partial t} = -\frac{\partial \Phi}{\partial y} + fv - u\frac{\partial u}{\partial x} - v\frac{\partial u}{\partial y}$$

$$\frac{\partial v}{\partial t} = -\frac{\partial \Phi}{\partial x} - fu - u\frac{\partial v}{\partial x} - v\frac{\partial v}{\partial y}, \tag{25}$$

where Φ is the geopotential height.

In the next section, we briefly present a case study of the application of Lighthill–Ford theory to clear-air turbulence forecasting as an illustration of the approach and its efficacy and as a prelude to its application on longer time scales.

4. Case study

On 9 March 2006, a significant CAT outbreak occurred over portions of the Upper Mississippi and Ohio Valleys. In 2 h between 0000 and 0200 UTC 10 March nearly three dozen pilot reports (PIREPs) of CAT were received, including eight reports of severe or moderate-to-severe turbulence. Most of the strongest turbulence was experienced in the upper troposphere above FL350, in convergent southwest flow ahead of a trough over the Great Plains (Fig. 1).

Using the 1-h Rapid Update Cycle (RUC) 2 forecast from 0000 UTC 10 March 2006, we calculate the TKE dissipation using (23) as the gravity wave forcing. Fig. 2a depicts 200–225-hPa TKE dissipation overlaid with PIREPs of turbulence occurring between FL350 and FL410. The agreement between regions of maximum TKE dissipation and PIREPs of turbulence is considerable, especially given the relative sparseness and inhomogeneity of pilot reports. Also of note is the null report of turbulence made in a region of minimal TKE dissipation rates. By comparison, the 25-hPa layer (200–225 hPa) bulk Richardson number (Fig. 2b) indicates very broad regions of $\mathrm{Ri} < 1$ across much of Illinois, southern Wisconsin, and parts of Michigan. This is the classic problem of overprediction of CAT that plagues most CAT forecast indicators. By contrast, Fig. 2b illustrates that leading- and second-order terms of Lighthill–Ford radiation correspond to better-defined regions of maxima than does Ri.

Cross sections during this CAT outbreak also reveal the efficacy of Lighthill–Ford theory in identifying

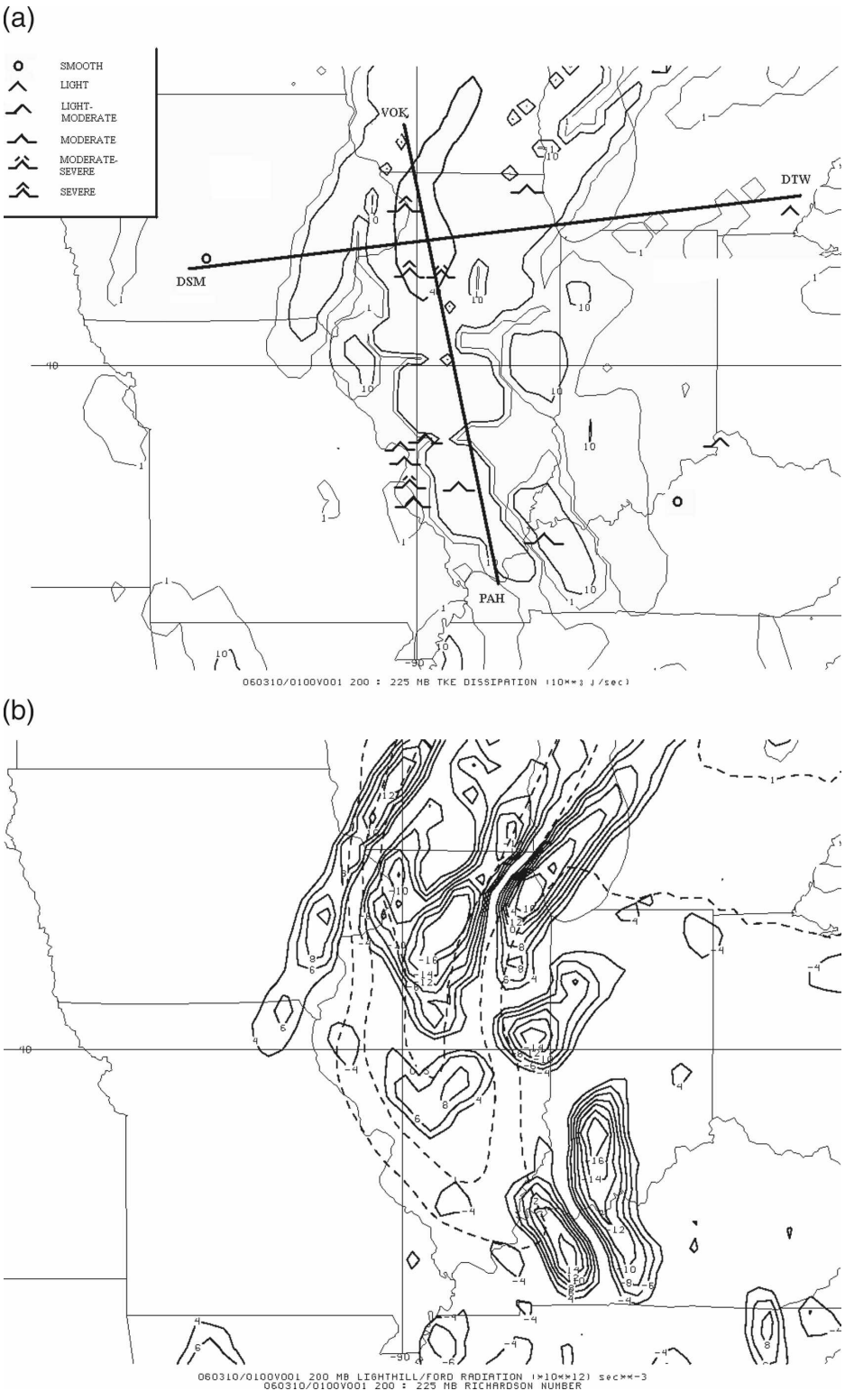

FIG. 2. (a) 200–225-hPa TKE dissipation overlaid with pilot reports of turbulence occurring over the Upper Mississippi and Ohio Valleys between FL350 and FL410 using the 1-h RUC2 forecast at 0000 UTC 10 Mar 2006. Lines indicate cross sections used in subsequent figures. (b) Lighthill–Ford radiation (solid lines) and 200–225-hPa Richardson number (dashed lines) for the same region and time period. The Lighthill–Ford radiation is calculated using the leading- and second-order terms determined in section 2 and the method described in section 3.

likely regions for turbulence. Figure 3 shows nearly perpendicular cross sections from Des Moines, Iowa (DSM), to Detroit, Michigan (DTW), and Volk Field, Camp Douglas, Wisconsin (VOK), to Paducah, Kentucky (PAH). PIREPs of turbulence within 100 km of the cross section are overlaid. The turbulence reports generally coincide with high values of TKE dissipation rate. Conversely, null reports of turbulence generally coincide with low values of TKE dissipation rate. Spatial patterns of ε using Lighthill–Ford theory are relatively coherent; that is, they more closely resemble the physical wave patterns found in experiments by Williams et al. (2005) than numerical noise.

The results of this case study support the notion that application of shallow-water Lighthill–Ford theory to the problem of clear-air turbulence could lead to beneficial forecasts of CAT, even in baroclinic situations. How does this approach fare over longer periods of time, and how does its accuracy compare to that of existing methods of CAT forecasting? We explore these questions in the next section.

5. Seasonal statistics

The method of CAT forecasting explicated in the preceding sections is now used to diagnose the occurrence of CAT during a 144-day period using the 20-km output from the 13-km RUC2 operational numerical weather prediction model. Layer TKE dissipation rates calculated from the 1-h forecasts from the 1500 UTC model run (valid at 1600 UTC) for each day from 3 November 2005 to 26 March 2006 are validated with 5546 text pilot reports of turbulence from 1500 to 1700 UTC at or above FL200. PIREPs of turbulence in convection (as determined subjectively from satellite imagery) or in mountain waves (as determined from the MWAVE algorithm; see McCann 2006) were not included in the database. The maximum TKE dissipation rate in the layer with the FL within 50 km of the pilot report of CAT was matched with the subjective pilot report of the intensity of the turbulence. [See Schwartz (1996) and Bass (2001) for a discussion of limitations and inconsistencies in these subjective reports.]

One way to assess an algorithm's skill is to create a set of 2×2 contingency tables by varying the threshold chosen to make a yes-or-no forecast decision and then comparing those with the yes-or-no observed conditions (Mason 1982). For each threshold the members of the table are the number of correct yes forecasts (YY), the number of correct no forecasts (NN), the number of incorrect yes forecasts (YN), and the number of missed forecasts (NY). The Heidke skill score (HSS; Doswell et al. 1990) is one of many skill summary measures for 2×2 contingency tables. It gives credit for the correct forecasts (YY and NN) and deducts for the incorrect forecasts (YN and NY). The score may vary between -1 and 1, with 0 meaning no skill. The HSS's strength over other summary measures is its ability to account for rare events. Because PIREPs are sparse and not random (they tend to report positive turbulence), the YN and NY categories may be uncertain. Therefore, the absolute value of the HSS is not likely accurate, but it may be compared within an HSS set to assess which threshold creates the highest skill.

Figure 4 shows the HSS for our application of Lighthill–Ford theory to CAT forecasting during November 2005–March 2006. It reveals a positive forecast skill for all CAT intensities. Especially noteworthy is that the highest score for the differentiation between no turbulence and positive turbulence is for a zero threshold. In other words, when there is a positive TKE dissipation forecast, aircraft will likely feel some turbulence. At moderate and severe intensities the HSS peaks with higher TKE dissipation; this indicates that the higher the forecast TKE rate, the stronger the expected turbulence. This is a very desirable feature of a CAT forecasting technique, given the practical importance of differentiating between various CAT intensities.

An alternative statistical analysis of forecasting is the receiver operating characteristic (ROC) curve. Popularized in the field of radiology (e.g., Hanley and McNeil 1982), a ROC graphic contains the YY percentage of total reports versus the NN percentage of total reports for a range of thresholds; collectively, this defines the ROC curve. Each point on the curve is the forecast's accuracy for a given threshold. The closer the ROC curve is to the upper-right corner of the graph, the more skillful the method.

Recently, Sharman et al. (2006) statistically combined the historically most useful CAT forecast methods into a single product called the Graphical Turbulence Guidance (GTG). Their combined approach verified better than any other single method. Figure 5 compares the ROC curve of our algorithm with the ROC curve of the current operational version of the GTG (GTG1) for moderate or greater turbulence during November 2005–March 2006. (The GTG curve in Fig. 5 is based on data obtained online at http://www.rtvs.noaa.gov.) As Fig. 5 illustrates, our approach over this period is more skillful than GTG for moderate or greater turbulence. Our approach is also more skillful than GTG for light or greater and severe turbulence (not shown). Because at the time of writing the GTG1 is currently the best available method, our results suggest that application of our approach to CAT forecast-

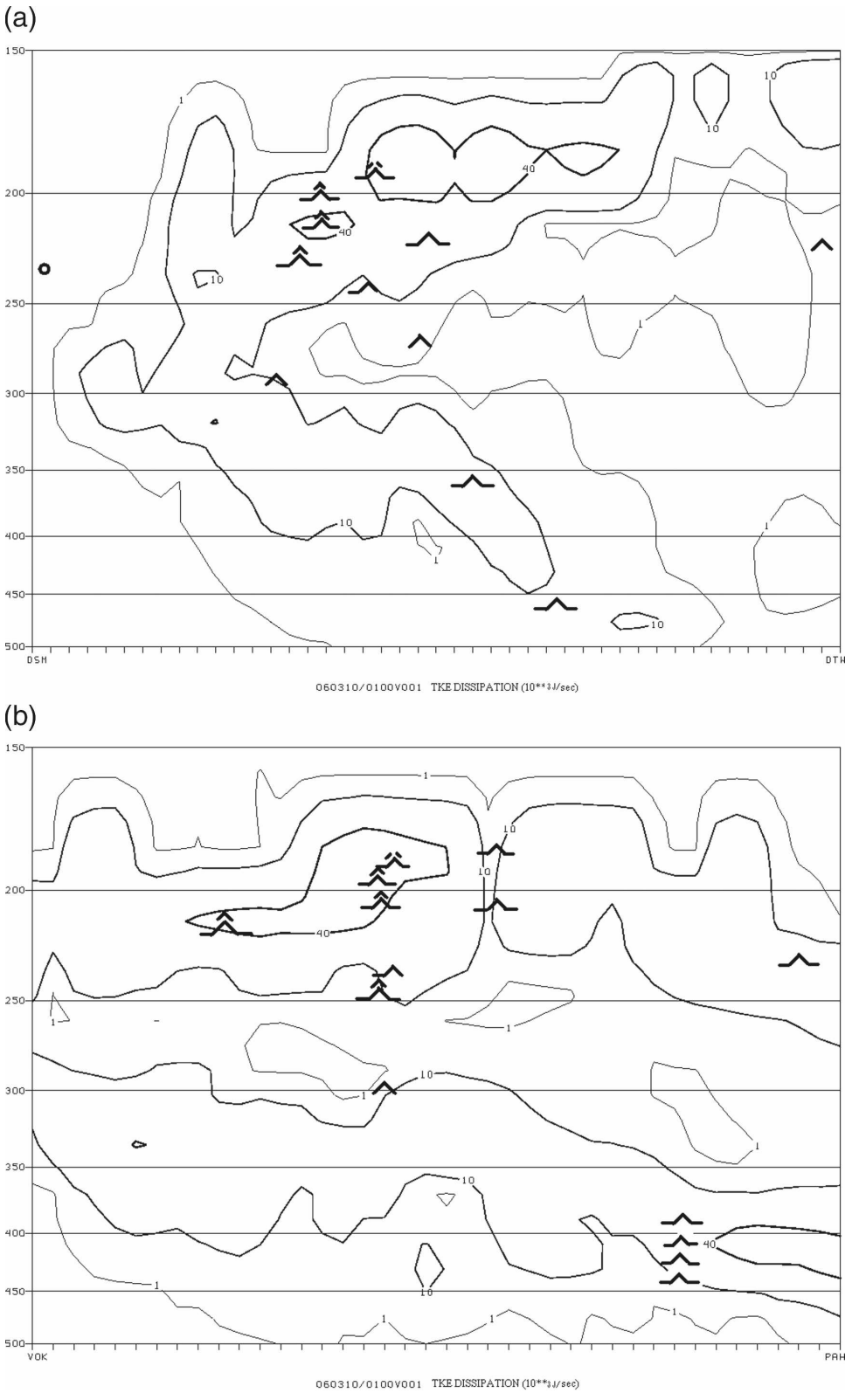

FIG. 3. (a) Vertical cross section from DSM to DTW of TKE dissipation using the 1-h RUC2 forecast at 0000 UTC 10 Mar 2006. PIREPs within 100 km of the cross section are overlaid. (b) As in (a), except for a vertical cross section from VOK to PAH. Symbols depicting pilot reports of turbulence are the same as in Fig. 2.

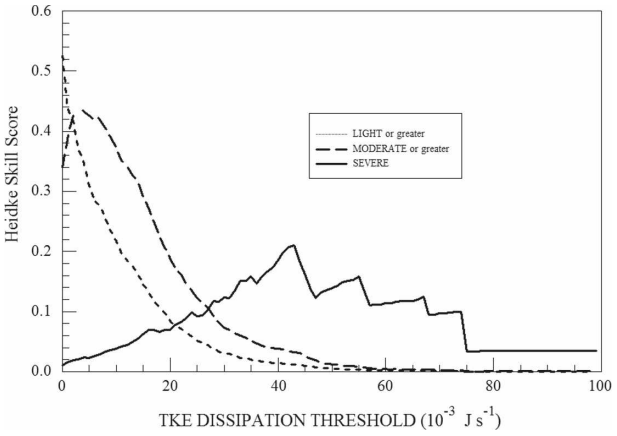

FIG. 4. HSS for various levels of clear-air turbulence using TKE dissipation based on Lighthill–Ford theory, for the 3 Nov 2005–26 Mar 2006 period. Layer TKE dissipation rates were calculated from the 1-h RUC2 forecasts from the 1500 UTC model run (valid at 1600 UTC) for each day, and validated with 5546 text pilot reports of turbulence from 1500 to 1700 UTC at or above FL200.

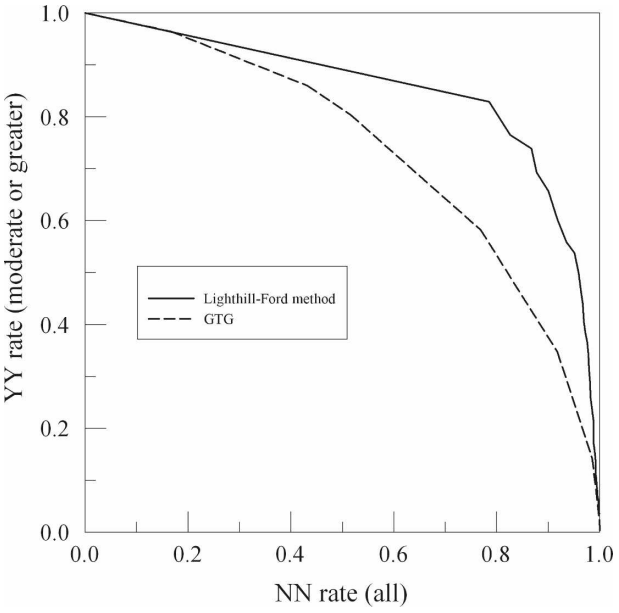

FIG. 5. ROC curves for the current operational GTG1 clear-air turbulence algorithm (dashed line) vs the Lighthill–Ford method (solid line) discussed in this paper. The closer that the ROC curve is to the upper-right corner of the graph, the more skillful the method.

ing could potentially be more skillful than the best methods typically used by forecasters today.[1]

The U.S. Federal Government's goal for CAT forecast techniques is for a probability of detection for moderate or greater turbulence greater than 0.8, with a probability of detection of null reports greater than 0.85 (Sharman et al. 2006). Based on the seasonal statistics shown in Fig. 5, our application is tantalizingly close to this goal, with a YY probability for moderate or greater turbulence of 0.829 and a NN probability for null turbulence of 0.785 at a zero threshold. However, at the most skillful threshold for moderate or greater turbulence the YY probability for our method is only 0.657.

6. Discussion and concluding remarks

In this paper, we have developed the Lighthill–Ford theory of spontaneous imbalance and gravity wave emission in a form amenable to clear-air turbulence forecasting. Using scale analysis, we have identified the main dynamical processes contributing to spontaneous imbalance for midlatitude synoptic-scale flows. In particular, we have singled out the leading-order contributor: the advection of relative vorticity. This may at least partly explain the observed relationship between sharp PV gradients and inertia–gravity wave generation noted by others (e.g., Viúdez and Dritschel 2006). This result is also consistent with the sometimes overlooked work of Medvedev and Gavrilov (1995) concerning inertia–gravity wave generation by quasigeostrophic background flows.

We have used this theory to scrutinize past CAT forecasting approaches. This is instructive because the origins of many CAT forecasting techniques are at least partly empirical. Our hope is that our approach may be used to place the subject of CAT forecasting on a firmer theoretical footing.

We have implemented the leading- and second-order terms of the Lighthill–Ford radiation term as a CAT forecasting method via the TKE approach of McCann (2001). Tests using a single case study suggest its utility, and further analysis confirms its superiority to other methods over a 144-day period. It should be stressed that comparison to the GTG1 algorithm is a strenuous "acid test": GTG combines a host of tried-and-true CAT forecasting methods based on differing dynamical assumptions, and uses weighting functions and tuning versus observations to achieve an optimal forecast approach. Our application is, in contrast, based on a single consistent theory of spontaneous imbalance, predicated on shallow-water theory, and uses no statistical optimization. Nevertheless, as Fig. 5 indicates, our approach is potentially a significant advance beyond GTG1.

Returning to theoretical considerations, the demon-

[1] It should be noted that GTG2, an improved version of Graphical Turbulence Guidance that is scheduled to be operational in September 2008, has a performance superior to that of GTG1 and similar to that shown for Lighthill–Ford in Fig. 5 (Sharman et al. 2006, their Fig. 5).

strated utility of Lighthill–Ford theory as a CAT forecasting technique is remarkable given the assumptions involved. We have made no attempt in this paper to extend the theory beyond rotating shallow-water flows, or to incorporate a nonzero background flow. Furthermore, the spontaneous-adjustment emission theory of Ford et al. (2000) assumes Rossby numbers greater than unity. Inertia–gravity waves generated by that mechanism are thought to be exponentially small in amplitude for small Rossby number flows (e.g., Plougonven et al. 2005). The relevance of the Lighthill mechanism to emission from large-scale geophysical flows has therefore been debated (Saujani and Shepherd 2002; Ford et al. 2002). However, the Lighthill–Ford source term appears in a renormalization theory that permits inertia–gravity waves that are not exponentially small, even at small Rossby numbers (T. W. N. Haine 2008, personal communication). The emitted waves are mathematically slaved to the vortical flow, but still are perfectly capable of generating clear-air turbulence. This gives added motivation for the approach we have taken in this paper.

Our work highlights the potential importance of spontaneous imbalance as a source of gravity wave activity in the atmosphere, a point also noted by Medvedev and Gavrilov (1995). Future work will seek to extend the theory beyond rotating shallow-water flows and to pursue applications beyond clear-air turbulence forecasting.

Acknowledgments. The authors gratefully acknowledge Gary Ellrod, Stephen Jascourt, Bob Sharman, and Steven Silberberg for their comments. Thanks also to Greg Thompson for providing text PIREPs. PDW is funded through a U.K. NERC Fellowship (NE/D009138/1). Partial funding for publication was provided by the UGA Department of Geography.

REFERENCES

Bass, E. J., 2001: Research looks at how pilots assess and respond to encounters with turbulence. *ICAO J.,* **56** (7), 12–14, 28.

Brown, R., 1973: New indices to locate clear-air turbulence. *Meteor. Mag.,* **102,** 347–361.

Cahn, A., 1945: An investigation of the free oscillations of a simple current system. *J. Meteor.,* **2,** 113–119.

Cornman, L. B., C. S. Morse, and G. Cunning, 1995: Real-time estimation of atmospheric turbulence severity from in-situ aircraft measurements. *J. Aircraft,* **32** (1), 171–177.

Doswell, C. A., III, R. Davies-Jones, and D. Keller, 1990: On summary measures of skill in rare event forecasting based on contingency tables. *Wea. Forecasting,* **5,** 576–585.

Dunkerton, T. J., 1997: Shear instability of internal inertia-gravity waves. *J. Atmos. Sci.,* **54,** 1628–1641.

Dutton, J. A., and H. A. Panofsky, 1970: Clear air turbulence: A mystery may be unfolding. *Science,* **167,** 937–944.

Dutton, M. J. O., 1980: Probability forecasts of clear-air turbulence based on numerical model output. *Meteor. Mag.,* **109,** 293–310.

Ellrod, G. P., and D. I. Knapp, 1992: An objective clear-air turbulence forecasting technique: Verification and operational use. *Wea. Forecasting,* **7,** 150–165.

——, P. F. Lester, and L. J. Ehernberger, 2003: Clear air turbulence. *Encyclopedia of the Atmospheric Sciences,* J. R. Holton, J. Pyle, and J. A. Curry, Eds., Academic Press, 393–403.

Ford, R., 1994: Gravity wave radiation from vortex trains in rotating shallow water. *J. Fluid Mech.,* **281,** 81–118.

——, M. E. McIntyre, and W. A. Norton, 2000: Balance and the slow quasimanifold: Some explicit results. *J. Atmos. Sci.,* **57,** 1236–1254.

——, ——, and ——, 2002: Reply. *J. Atmos. Sci.,* **59,** 2878–2882.

Haltiner, G. J., and R. T. Williams, 1980: *Numerical Prediction and Dynamic Meteorology*. John Wiley & Sons, 477 pp.

Hanley, J., and B. McNeil, 1982: The meaning and use of the area under the receiver operating characteristic (ROC) curve. *Radiology,* **132,** 29–36.

Houghton, D. D., W. H. Campbell, and N. D. Reynolds, 1981: Isolation of the gravity-inertial motion component in a nonlinear atmospheric model. *Mon. Wea. Rev.,* **109,** 2118–2130.

Kaplan, M. L., A. W. Huffman, K. M. Lux, J. J. Charney, A. J. Riordan, and Y.-L. Lin, 2005: Characterizing the severe turbulence environments associated with commercial aviation accidents. Part I: A 44 case study synoptic observational analyses. *Meteor. Atmos. Phys.,* **88,** 129–152.

Keller, J. L., 1990: Clear air turbulence as a response to meso- and synoptic-scale dynamic processes. *Mon. Wea. Rev.,* **118,** 2228–2242.

Knox, J. A., 1997: Possible mechanisms of clear-air turbulence in strongly anticyclonic flow. *Mon. Wea. Rev.,* **125,** 1251–1259.

——, 2001: The breakdown of balance in low potential vorticity regions: Evidence from a clear air turbulence outbreak. Preprints, *13th Conf. on Atmospheric and Oceanic Fluid Dynamics,* Breckenridge, CO, Amer. Meteor. Soc., 64–67.

Koch, S. E., and P. B. Dorian, 1988: A mesoscale gravity wave event observed during CCOPE. Part III: Wave environment and probable source mechanisms. *Mon. Wea. Rev.,* **116,** 2570–2592.

Lighthill, M. J., 1952: On sound generated aerodynamically, I. General theory. *Proc. Roy. Soc. London,* **211A,** 564–587.

Mancuso, R. L., and R. M. Endlich, 1966: Clear air turbulence frequency as a function of wind shear and deformation. *Mon. Wea. Rev.,* **94,** 581–585.

Mason, L., 1982: A model for assessment of weather forecasts. *Aust. Meteor. Mag.,* **30,** 291–303.

McCann, D. W., 1999: A simple turbulent kinetic energy equation and aircraft boundary layer turbulence. *Natl. Wea. Dig.,* **23** (1–2), 13–19.

——, 2001: Gravity waves, unbalanced flow, and clear air turbulence. *Natl. Wea. Dig.,* **25** (1–2), 3–14.

——, 2006: Diagnosing and forecasting aircraft turbulence with steepening mountain waves. *Natl. Wea. Dig.,* **30,** 77–92.

Medvedev, A. S., and N. M. Gavrilov, 1995: The nonlinear mechanism of gravity wave generation by meteorological motions in the atmosphere. *J. Atmos. Terr. Phys.,* **57,** 1221–1231.

Miles, J. W., and L. N. Howard, 1964: Note on a heterogeneous shear flow. *J. Fluid Mech.,* **20,** 331–336.

Moore, J. T., and W. A. Abeling, 1988: A diagnosis of unbalanced flow in upper levels during the AVE—SESAME I period. *Mon. Wea. Rev.,* **116,** 2425–2436.

Nappo, C. J., 2003: *An Introduction to Atmospheric Gravity Waves*. Academic Press, 276 pp.

Plougonven, R., and F. Zhang, 2007: On the forcing of inertia-gravity waves by synoptic-scale flows. *J. Atmos. Sci.,* **64,** 1737–1742.

——, D. J. Muraki, and C. Snyder, 2005: A baroclinic instability that couples balanced motions and gravity waves. *J. Atmos. Sci.,* **62,** 1545–1559.

Reznik, G. M., V. Zeitlin, and M. Ben Jelloul, 2001: Nonlinear theory of geostrophic adjustment. Part 1. Rotating shallow-water model. *J. Fluid Mech.,* **445,** 93–120.

Roach, W. T., 1970: On the influence of synoptic development on the production of high level turbulence. *Quart. J. Roy. Meteor. Soc.,* **96,** 413–429.

Rossby, C.-G., 1938: On the mutual adjustment of pressure and velocity distributions in certain simple current systems II. *J. Mar. Res.,* **2,** 239–263.

Saujani, S., and T. G. Shepherd, 2002: Comments on "Balance and the slow quasimanifold: some explicit results." *J. Atmos. Sci.,* **59,** 2874–2877.

Schwartz, B., 1996: The quantitative use of PIREPs in developing aviation weather guidance products. *Wea. Forecasting,* **11,** 372–384.

Shapiro, M. A., 1978: Further evidence of the mesoscale and turbulent structure of upper level jet stream–frontal zone systems. *Mon. Wea. Rev.,* **106,** 1100–1111.

Sharman, R., C. Tebaldi, G. Wiener, and J. Wolff, 2006: An integrated approach to mid- and upper-level turbulence forecasting. *Wea. Forecasting,* **21,** 268–287.

Smith, R. B., 1979: The influence of mountains on the atmosphere. *Advances in Geophysics,* Vol. 21, Academic Press, 87–230.

Sorenson, J. E., 1964: Synoptic patterns for clear air turbulence. UAL Meteorology Circular 56, 64 pp. [Available from Dept. of Atmospheric Science, Colorado State University, Fort Collins, CO 80523.]

Sparks, W. R., S. G. Cornford, and J. K. Gibson, 1977: *Bumpiness in Clear Air and Its Relation to Some Synoptic-Scale Indices.* Geophysical Memoirs Series, Vol. 121, Met Office, 53 pp.

Sugimoto, N., K. Ishioka, and K. Ishii, 2008: Parameter sweep experiments on spontaneous gravity wave radiation from unsteady rotational flow in an *f*-plane shallow water system. *J. Atmos. Sci.,* **65,** 235–249.

Uccellini, L. W., P. J. Kocin, R. A. Petersen, C. H. Wash, and K. F. Brill, 1984: The President's Day cyclone of 18–19 February 1979: Synoptic overview and analysis of the subtropical jet streak influencing the pre-cyclogenetic period. *Mon. Wea. Rev.,* **112,** 31–55.

van Tuyl, A. H., and J. A. Young, 1982: Numerical simulation of nonlinear jet streak adjustment. *Mon. Wea. Rev.,* **110,** 2038–2054.

Viúdez, Á., and D. G. Dritschel, 2006: Spontaneous generation of inertia-gravity wave packets by balanced geophysical flows. *J. Fluid Mech.,* **553,** 107–117.

Williams, P. D., P. L. Read, and T. W. N. Haine, 2003: Spontaneous generation and impact of inertia-gravity waves in a stratified, two-layer shear flow. *Geophys. Res. Lett.,* **30,** 2255, doi:10.1029/2003GL018498.

——, T. W. N. Haine, and P. L. Read, 2005: On the generation mechanisms of short-scale unbalanced modes in rotating two-layer flows with vertical shear. *J. Fluid Mech.,* **528,** 1–22.

——, ——, and ——, 2008: Inertia–gravity waves emitted from balanced flow: Observations, properties, and consequences. *J. Atmos. Sci.,* in press.

Zhang, F., S. E. Koch, C. A. Davis, and M. L. Kaplan, 2000: A survey of unbalanced flow diagnostics and their applications. *Adv. Atmos. Sci.,* **17,** 1–19.